A Control Strategy for Four-Switch Three-Phase Brushless DC Motor Using Single Current Sensor

Changliang Xia, *Member, IEEE*, Zhiqiang Li, and Tingna Shi

***Abstract*—A control strategy based on single current sensor is proposed for a four-switch three-phase brushless dc (BLDC) motor system to lower cost and improve performance. The system's whole working process is divided into two groups. In modes 2, 3, 5, and 6, where phase *c* works, phase-*c* current is sensed to control phases *a* and *b*, and phase-*c* current is consequently regulated. In modes 1 and 4, the combination of four suboperating modes for controlling phase-*c* current is proposed based on detailed analysis on the different rules that these operating modes have on phase-*c* current. Phase-*c* current is maintained at nearly zero level first, and phase-*a* and phase-*b* currents are regulated by speed circle. To improve control performance, a single-neuron adaptive proportional–integral (PI) algorithm is adopted to realize the speed regulator. Simulation and experimental systems are set up to verify the proposed strategy. According to simulation and experimental results, the proposed strategy shows good self-adapted track ability with low current ripple and strong robustness to the given speed reference model. Also, the structure of the drive is simplified.**

***Index Terms*—Brushless dc (BLDC) motor, four-switch three-phase inverter, single-neuron adaptive proportional–integral (PI) controller.**

I. Introduction

As BRUSHLESS dc (BLDC) motors have such good features as simple construction, high reliability, light electromagnetic pollution, and high power density, they are used extensively in servo systems and low-power drive systems [1], [2]. The performance of such motors has been significantly improved due to great development of power electronics, microelectronics, magnetic performance of magnets, and motion control technology in recent years [3]–[8]. Nowadays, many studies have been focused on how to reduce the cost of the BLDC motor and its control system without performance degradation [9]–[14].

A novel four-switch three-phase BLDC motor drive is proposed to simplify the topological structure of the conventional six-switch inverter. It is an effective try on reducing cost, but the uncontrollable phase current causes unsymmetrical voltage vector, and its waveform is much of distortion from rectangular. The direct current control based on hysteresis avoids this problem, and it senses currents of phases *a* and *b* individually by two current sensors and then switches them separately. Therefore, the desired rectangular current waveform is directly obtained [15]. In [16], a new speed control method using the acceleration feedforward compensation is proposed to improve the speed response characteristic for a four-switch three-phase BLDC motor. The disturbance torque estimation method is adopted to improve the robustness of the method. It is verified to be economical and efficient in some occasions with light load, such as robot arm, in spite of its average control performance with heavy load. Reference [17] presents an original study on the generated torque ripples due to phase commutation in the four-switch three-phase BLDC motor. A current control technique is developed to minimize commutation torque for the entire speed range. Its dynamic and static speed–torque characteristics are proved to be quite good. Intelligent schemes have been introduced into four-switch drives. An adaptive neuro-fuzzy inference system controller is proposed in [18]. This newly developed design does not require an accurate model of the motor and has a fairly simple structure. Simulation results show better transient and steady-state responses compared with the proportional–integral (PI) controller in the wide speed range. Some work has also been done on a sensorless four-switch BLDC motor drive [19], [20]. Reference [19] proposes an asymmetric PWM scheme for a four-switch three-phase BLDC motor drive to make six commutations and produce four floating phases to detect back electromotive force (back-EMF). The position information of the rotor can be acquired based on the crossing points of the voltage of controllable phases. In [20], virtual Hall sensor signals are made by detecting the zero crossing points of the stator terminal voltages, and there is no need to build a 30° phase shift, which is prevalent in most of the sensorless algorithms.

The aforementioned research works are all based on two current sensors. To exploit the four-switch BLDC motor drive's advantage of lower cost, a single-current-sensor control strategy is proposed in this paper. The designed four-switch BLDC motor drive shows satisfying performance despite the reduction of current sensor. In Section II, how variation of phase-*c* current i_c influences another phase currents is analyzed, and the four-switch control strategy based on i_c is proposed. Section III introduces a single-neuron adaptive PI algorithm to the speed regulator to improve control performance and demonstrates implementation of the control system in detail. Finally, simulation and experimental results are given in Section IV.

II. Four-Switch Three-Phase BLDC Motor Control Based on Phase *C* Current

Fig. 1 shows the configuration of a four-switch inverter for the three-phase BLDC motor.

Manuscript received July 22, 2008; revised January 15, 2009. First published February 6, 2009; current version published June 3, 2009. This work was supported by Scientific Funds for Outstanding Young Scientists of China under Grant 50825701.

The authors are with the School of Electrical Engineering and Automation, Tianjin University, Tianjin 300072, China (e-mail: yiruwangxi@yeah.net).

Digital Object Identifier 10.1109/TIE.2009.2014307

0278-0046/$25.00 © 2009 IEEE

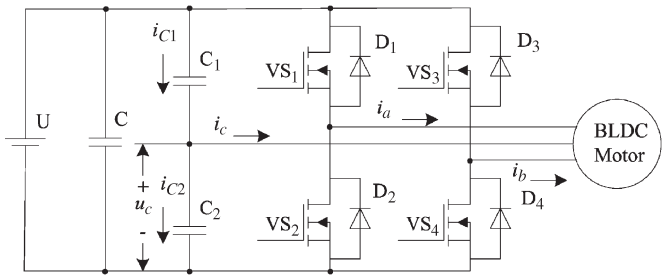

Fig. 1. Four-switch three-phase inverter.

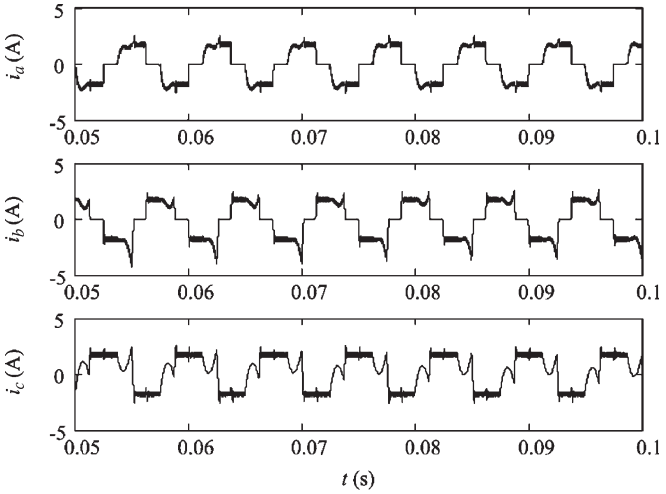

Fig. 2. Phase current waveforms when the four-switch three-phase BLDC motor is controlled by the six-switch three-phase strategy.

As shown in Fig. 1, two common capacitors, instead of a pair of bridges, are used, and phase *c* is out of control because it is connected to the midpoint of the series capacitors. A conventional PWM scheme for the six-switch inverter is used for the four-switch inverter topology of the BLDC motor drive, and its phase current waveforms are shown in Fig. 2.

From Fig. 2, it is noted that i_c cannot hold at zero, and it causes an additional and unexpected current, resulting in current distortion in phases *a* and *b*, and even in the breakdown of the system. The same problem is inherited by the four-switch mode, and it causes the produced voltage vectors to be limited and asymmetric, which were well known as "asymmetric voltage vectors."

The BLDC motor needs quasi-square current waveforms, which are synchronized with the back-EMF to generate constant output torque and have 120° conducting and 60° nonconducting regions. Also, at every instant, only two phases are conductive, and the other phase is inactive.

Compared with the conventional six-switch three-phase inverter for the BLDC motor, the whole working process of the BLDC motor is divided into six modes, as shown in Table I.

Phase *c* involves four modes, including modes 2, 3, 5, and 6. Only one switch should work in the four modes. Taking mode 2 for instance, switch VS_1 and diode D_2 work to conduct current in this mode. Mode 2 is divided into modes 21 and 22, as shown in Fig. 3. Switch VS_1 turns on, while $-i_c$ is less than current threshold I^*. As $i_c = -(i_a + i_b)$ and the current flows through only two phases, i_a increases and $i_b = 0$. Then, i_c is controlled

TABLE I
WORKING MODE OF THE FOUR-SWITCH THREE-PHASE BLDC MOTOR

Mode	Hall values	Working phase	Current restraint	Conducting devices
Mode 1	101	+a,-b	$i_a=I^*$, $i_b=-I^*$	VS_1, VS_4
Mode 2	100	+a,-c	$i_a=I^*$	VS_1
Mode 3	110	+b,-c	$i_b=I^*$	VS_3
Mode 4	010	+b,-a	$i_b=I^*$, $i_a=-I^*$	VS_2, VS_3
Mode 5	011	+c,-a	$i_a=-I^*$	VS_2
Mode 6	001	+c,-b	$i_b=-I^*$	VS_4

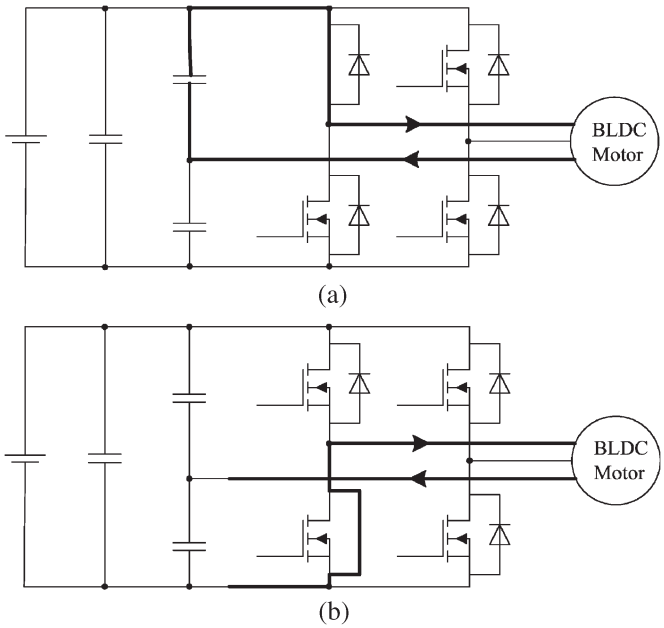

Fig. 3. Suboperating modes of mode 2. (a) Mode 21. (b) Mode 22.

indirectly. While $-i_c$ goes beyond I^*, switch VS_1 turns off, and diode D_2 conducts to make i_a and $-i_c$ drop. In this way, i_a and i_c are regulated to vary near the reference value.

As far as the situation of modes 1 and 4 is concerned, phases *a* and *b* have current flowing through, and i_c should be zero. To avoid current waveform distortion, appropriate switch signals should be respectively used in different working modes, which implies that some new control schemes should be developed.

Considering three balanced phase windings, assuming that the performance of power devices of the inverter is ideal, and ignoring armature reaction, slot effect, and iron losses, the voltage equations for a three-phase BLDC motor can be described as

$$u_x = i_x R + L\frac{di_x}{dt} + e_x + u_N, \qquad x = a, b, c \tag{1}$$

where u_x represents the terminal phase voltage with respect to power ground, i_x is the rectangular-shaped phase current, e_x is the trapezoidal-shaped back-EMF, u_N is the neutral-point voltage with respect to power ground, and R and L are the resistance and equivalent inductance of the phase windings, respectively.

As

$$i_a + i_b + i_c = 0 \tag{2}$$

(3) can be drawn from (1) and (2)

$$Ri_c + L\frac{di_c}{dt} - \frac{2}{3}u_c + \left(\frac{2}{3}e_c + \frac{u_a + u_b}{3}\right) = 0 \tag{3}$$

considering that

$$i_c = i_{C1} - i_{C2} \tag{4}$$

$$i_{C1} = C\frac{d(U - u_c)}{dt} \tag{5}$$

$$i_{C2} = C\frac{du_c}{dt} \tag{6}$$

so

$$i_c = -2C\frac{du_c}{dt} \tag{7}$$

where C represents the value of capacitors of C_1 and C_2 and U is the dc-link voltage.

Equation (3) can be rewritten as follows, in which u_c is the only argument:

$$2LC\frac{d^2u_c}{dt^2} + 2RC\frac{du_c}{dt} + \frac{2}{3}u_c - \left(\frac{2}{3}e_c + \frac{u_a + u_b}{3}\right) = 0. \tag{8}$$

Assuming that $e_c = e_0$ at some instant, $-E < e_0 < E$, where E is the amplitude of the back-EMF. At the instant of $t = 0$, $i_c(0)$ is assumed to be equal to i_0 and $i_0 \approx 0$. If the value of capacitors is large enough, then $u_c(0) = U/2 + u_0$ and $u_0 \approx 0$.

Considering the case of $\Delta = 4R^2C^2 - 16LC/3 > 0$ as an example, i_c and u_c can be resolved from (7) and (8), respectively,

$$u_c = \frac{3L(BCr_2 - i_0)e^{r_1 t} - 3L(BCr_1 - i_0)e^{r_2 t}}{2\sqrt{9R^2C^2 - 12LC}} + \frac{2e_0 + u_a + u_b}{2} \tag{9}$$

$$i_c = \frac{-3LC(BCr_2 - i_0)r_1 e^{r_1 t} + 3LC(BCr_1 - i_0)r_2 e^{r_2 t}}{\sqrt{9R^2C^2 - 12LC}}. \tag{10}$$

To simplify the results, several variables B, r_1, and r_2 are declared as

$$B = u_a + u_b + 2e_c - 2u_0 - U \tag{11}$$

$$r_1 = (\sqrt{9R^2C^2 - 12LC} - 3RC)/(6LC) \tag{12}$$

$$r_2 = (-\sqrt{9R^2C^2 - 12LC} - 3RC)/(6LC). \tag{13}$$

The variance ratio of i_c is

$$\frac{di_c}{dt} = \frac{-3LC(BCr_2 - i_0)r_1^2 e^{r_1 t} + 3LC(BCr_1 - i_0)r_2^2 e^{r_2 t}}{\sqrt{9R^2C^2 - 12LC}}. \tag{14}$$

The Taylor series of di_c/dt at the instant $t = 0$ can be solved, and all items that are more than one degree are truncated. Then,

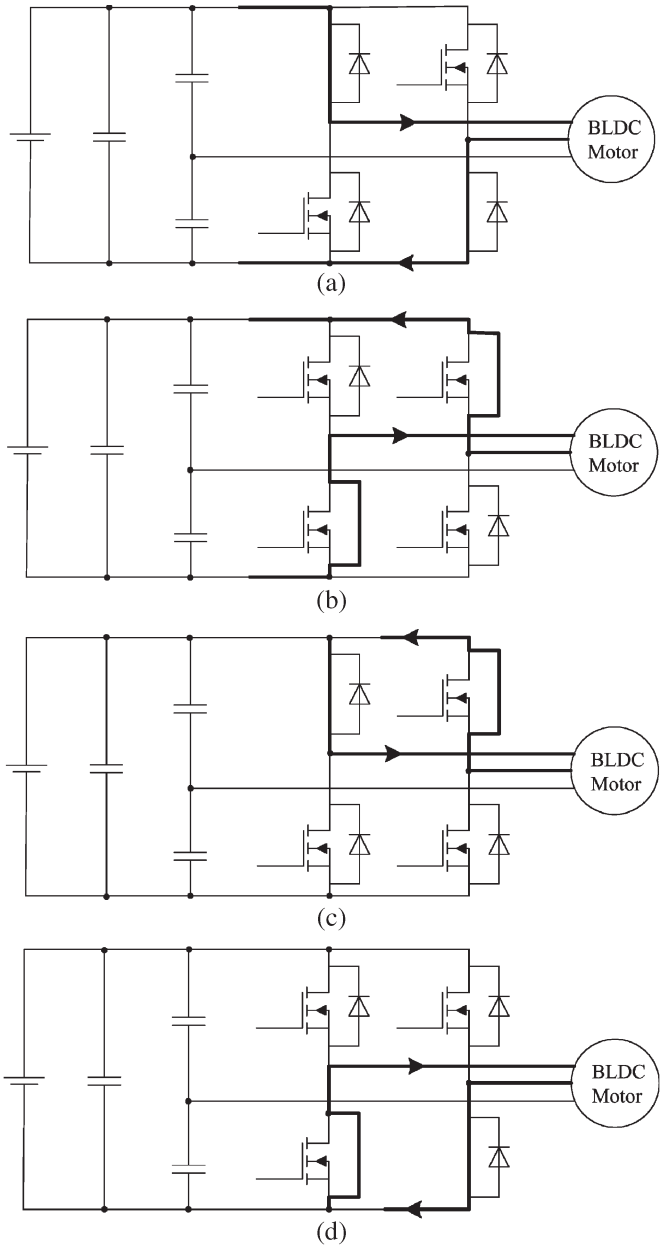

Fig. 4. Suboperating modes of mode 1. (a) Mode 11. (b) Mode 12. (c) Mode 13. (d) Mode 14.

the variance ratio of i_c at $t = 0$ is

$$\frac{di_c}{dt}(0) = \frac{2u_0 - 3Ri_0 + U - u_a - u_b - 2e_0}{3L} \approx \frac{U - u_a - u_b - 2e_0}{3L}. \tag{15}$$

Mode 1 is taken for instance here to demonstrate the whole working process that is identical in mode 4. Mode 1 is divided into four suboperating modes, i.e., modes 11, 12, 13, and 14, as shown in Fig. 4.

Switches VS_1 and VS_4 work in mode 11 with $u_a = U$ and $u_b = 0$. Diodes D_2 and D_3 work in mode 12 with $u_a = 0$ and $u_b = U$. Switch VS_1 and diode D_3 work in mode 13 with $u_a = U$ and $u_b = U$. Switch VS_4 and diode D_2 work in mode 14 with

TABLE II
$di_c/dt(t=0)$ IN SUBOPERATING MODES

Sub-operating Mode	u_a	u_b	$di_c/dt\ (t=0)$
Mode 11	U	0	$-2e_0/3L$
Mode 12	0	U	$-2e_0/3L$
Mode 13	U	U	$(-U-2e_0)/3L$
Mode 14	0	0	$(U-2e_0)/3L$

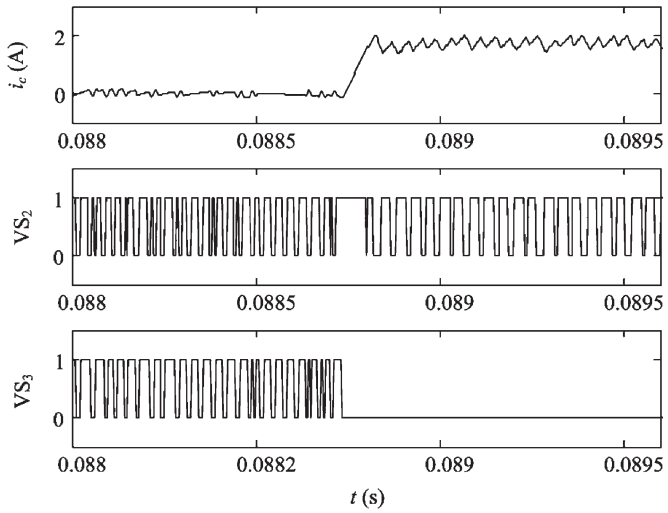

Fig. 5. Detailed phase current and switch signal.

$u_a = 0$ and $u_b = 0$. The values of $di_c/dt(t=0)$ in different suboperating modes are shown in Table II.

According to Table II, the four suboperating modes have different rules to phase current. In mode 11, i_a and $-i_b$ rise quickly, and i_c varies proportionally with the back-EMF of phase c. In mode 12, i_a and $-i_b$ drop quickly, and i_c changes proportionally with the back-EMF of phase c. Compared with modes 11 and 12, i_c falls much quicker in mode 13 and rises much quicker in mode 14. Identical conclusion can be drawn in the cases of $\Delta = 0$ and $\Delta < 0$.

Thus, mode 1 could be optimized by reasonable combination of four suboperating modes. First of all, the equation $i_c = 0$ must be satisfied to keep the system stable as follows.

When i_c deviates seriously from zero, modes 13 and 14 work. When i_c remains at zero, modes 11 and 12 work. Because i_a and i_b cannot be detected, a speed loop is used here to decide the duty of PWM signals.

The same regulating method is used in mode 4, and asymmetric voltage vectors are eliminated. The detailed phase current and switch signals are shown in Fig. 5.

The corresponding Hall signals, switch signals, and waveforms of phase currents are shown in Fig. 6.

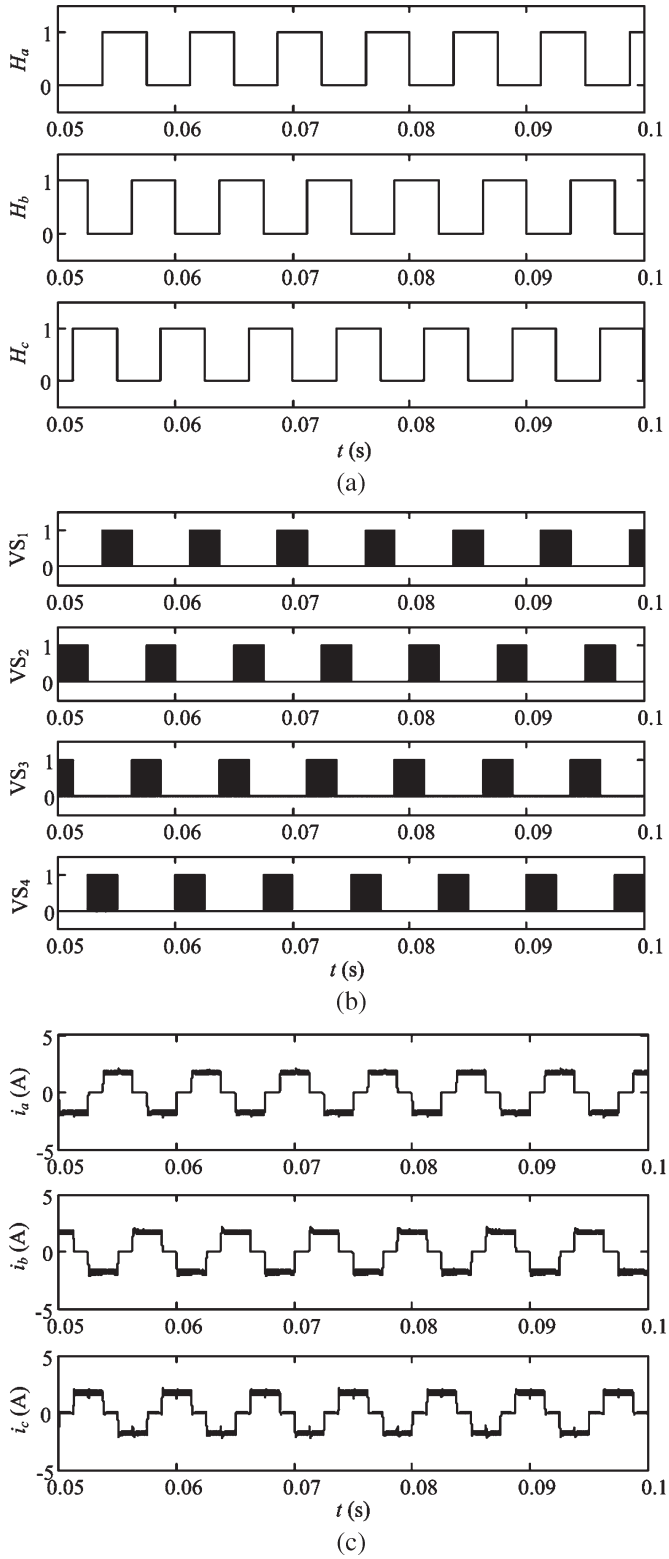

Fig. 6. Waveforms when the four-switch BLDC motor is controlled by the single-current-sensor strategy. (a) Hall signals. (b) Switch signals. (c) Current waveforms.

III. IMPLEMENTATION OF SINGLE-CURRENT-SENSOR CONTROL FOR FOUR-SWITCH THREE-PHASE BLDC MOTOR

A. Single-Neuron Adaptive PI Controller

Due to its merits such as simple structure, high efficiency, and easy implementation, the PI controller is widely used in most servo applications such as actuation, robotics, machine tools, and so on. However, the conventional PI controller is based on a linear model and suffers from parameter sensitivity and nonlinearity of the BLDC motor. Its accuracy is limited on BLDC motor control.

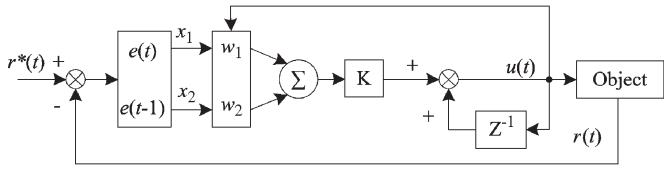

Fig. 7. Schematic of the single-neuron adaptive PI controller.

With the development of modern computer technology and control theory, new controllers are designed by not only combining the traditional PI strategy with some intelligent technologies but also adjusting PI controllers' parameters, so PI controllers' characteristics are improved greatly. The single-neuron adaptive PI controller is one of those controllers.

Neuron is the basic computing unit of the brain. It works as accumulative information processing properties. A single-neuron model is proposed based on the fact that the output of the neuron is the weighted sum of all the signals coming to it. The advantage of the single-neuron model is its adaptation ability acquired by adjusting the weigh coefficients.

Based on the self-study and adaptive ability of the single neuron, a single-neuron adaptive PI controller has the advantages of simple structure, fast response, good adaptability, and robustness [21], [22] and is consequently chosen as the speed controller in this paper. The structure of the single-neuron adaptive PI controller is shown in Fig. 7.

The regulating rule of the single-neuron adaptive PI controller can be described as follows.

1) Given the initial weight and learning rate of a single neuron, incremental PI controllers are used here, and the control error is

$$e(t) = r^*(t) - r(t) \tag{16}$$

where $r^*(t)$ is the threshold value at time t and $r(t)$ is the output of the system at time t.

2) The inputs of the single-neuron adaptive PI controller are

$$x_1(t) = e(t) \tag{17}$$

$$x_2(t) = e(t) - e(t-1). \tag{18}$$

3) The output of the single-neuron adaptive PI controller is

$$u(t) = u(t-1) + K \sum_{i=1}^{2} \left(x_i(t) w_i(t)\right) / \sum_{i=1}^{2} |w_i(t)| \tag{19}$$

where $w_i(t)$ is the corresponding weight of $x_i(t)$, and K is the learning rate of a neuron, with $K > 0$.

4) The weight coefficients of a single neuron are tuned by

$$w_1(t) = w_1(t-1) + \eta_I e(t) u(t) x_1(t) \tag{20}$$

$$w_2(t) = w_2(t-1) + \eta_P e(t) u(t) x_2(t) \tag{21}$$

where η_P and η_I are the learning rates of proportion and integration, respectively. They are set to different values, so different weight coefficients can be tuned.

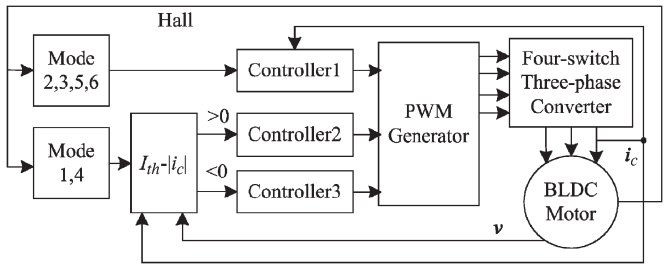

Fig. 8. Schematic of the controller.

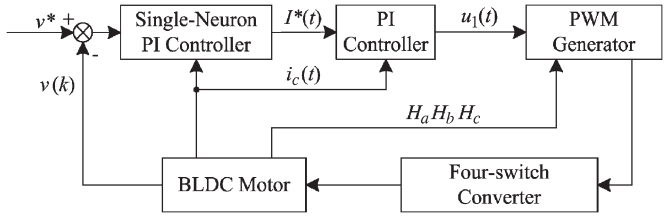

Fig. 9. Schematic of controller 1.

B. Control System

The control system adopts the double-loop structure. The inner current loop maintains the rectangular current waveforms, limits the maximum current, and ensures the stability of the system. The outer speed loop is designed to improve the static and dynamic characteristics of the system.

As the system performance is decided by the outer loop, the disturbance caused by the inner loop can be limited by the outer loop. Thus, the current loop adopts the conventional PI controller, and the speed loop adopts the single-neuron adaptive PI controller. Then, the parameter can be regulated online, and the system is adaptable to different working conditions. The whole system is shown in Fig. 8.

Controller 1: According to Hall signals, controller 1 works when the motor runs at modes 2, 3, 5, and 6. The scheme of controller 1 is shown in Fig. 9.

The single-neuron adaptive PI controller is taken as a speed controller. The speed difference can be represented as

$$e(t) = v^* - v(t) \tag{22}$$

where v^* is the given speed value and $v(t)$ is the measured speed value at time t.

The output of the single-neuron adaptive PI controller $I^*(t)$ can be solved by (16)–(21). $I^*(t)$ is the threshold value of the current regulator. For the safety of the system, $I^*(t)$ cannot pass beyond the maximum setting value.

Then, the input of the current regulator is

$$e_i(t) = I^*(t) - i_c(t). \tag{23}$$

An incremental PI controller is used here as a current regulator, and its output is

$$\Delta u_1(t) = k_{ip}\left(e_i(t) - e_i(t-1)\right) + k_{ii} e_i(t) T \tag{24}$$

where T represents the sampling period and k_{ip} and k_{ii} are the factors of proportion and integration of the current PI regulator, respectively.

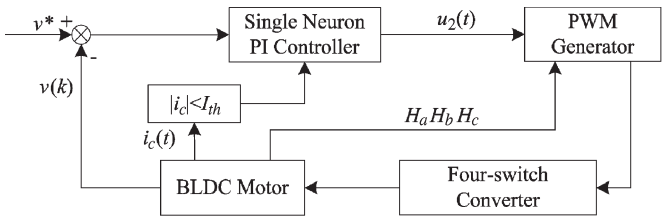

Fig. 10. Schematic of controller 2.

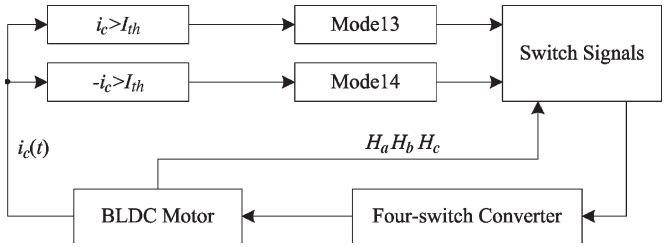

Fig. 11. Schematic of controller 3.

$u_1(t)$ is the duty of PWM signals.

Controller 2: In modes 1 and 4, $I_{\rm th}$ is close to zero. When $|i_c| < I_{th}$, i_c is regarded as equal to zero, and consequently, $i_a = -i_b$. Controller 2 works at this stage, and phases *a* and *b* switch synchronously based on the speed loop, just as the traditional six-switch method does, as shown in Fig. 10.

The input of controller 2 is

$$e(t) = v^* - v(k). \tag{25}$$

According to (16)–(21), the duty of PWM signals can be solved.

Controller 3: When the motor runs at modes 1 and 4, and $I_{\rm th} - |i_c| < 0$, controller 3 works, in turn, instead of controller 2, as shown in Fig. 11.

When $i_c > 0$ and $i_c > I_{\rm th}$, the strategy is at the stage of suboperating mode 13, and the magnitude of i_c drops quickly. If $i_c = 0$, the control flow will quit from controller 3. When $i_c < 0$ and $-i_c > I_{\rm th}$, the strategy is at the stage of suboperating mode 14, and the magnitude of i_c rises quickly. If $i_c = 0$, the control flow will quit from controller 3. Above all, the function of controller 3 is to keep $i_c = 0$. The adjustment to working phase current should be done by controller 2 after controller 3 quits.

IV. Simulation and Experimental Results

To verify the correctness and feasibility of the proposed strategy for the four-switch three-phase BLDC motor, a complete simulation system was built. The simulation results are compared with those of the six-switch speed PI controller.

The parameters of the BLDC motor are as follows: pole pairs $p = 4$, rated voltage $U_N = 36$ V, rated torque $T_N = 0.4$ N · m, rated speed $n_N = 3600$ r/min, equivalent inductance $L - M = 1.4$ mH($\pm 1.3\%$), back-EMF constant $K_e = 0.067$ V/(rad/s), and rotational inertia coefficient $J = 1.57 \times 10^{-5}$ kg · m^2.

The motor starts up with a speed reference of 300 r/min and a load of 0.1 N · m. At 0.04 and 0.07 s, the speed reference and load step to the rated ones, respectively. Simulation results

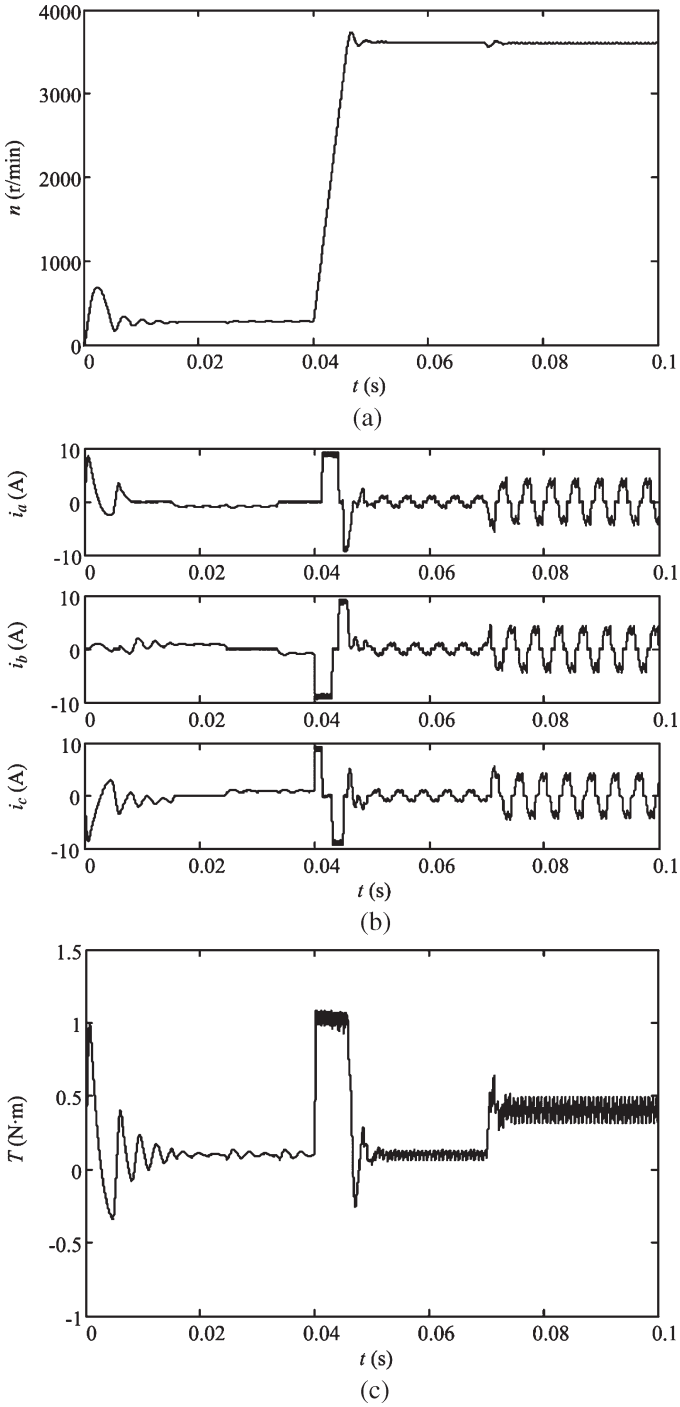

Fig. 12. Simulation waveforms when the motor is controlled by the conventional six-switch strategy. (a) Speed curve. (b) Current waveforms. (c) Torque curve.

of speed and phase current waveform are shown in Figs. 12 and 13.

From Figs. 12 and 13, compared with the conventional six-switch three-phase strategy, it can be seen that when the motor is controlled by the four-switch and single-current-sensor strategy, overshot is reduced at both low- and high-speed references. Adjusting time is also short. Speed curves show only slight ripples under load disturbance. Current waveforms are close to ideal trapezoidal form, and torque remains stable.

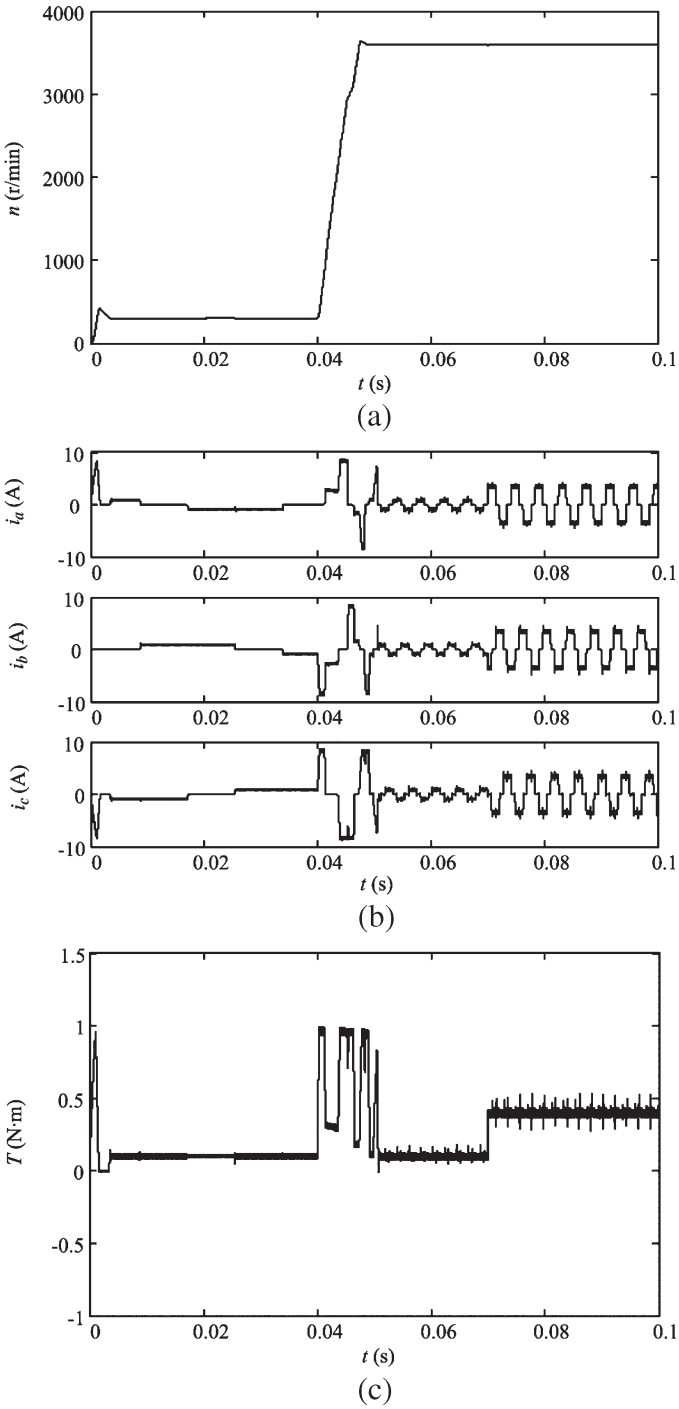

Fig. 13. Simulation waveforms when the motor is controlled by the single-current-sensor strategy. (a) Speed curve. (b) Current waveforms. (c) Torque curve.

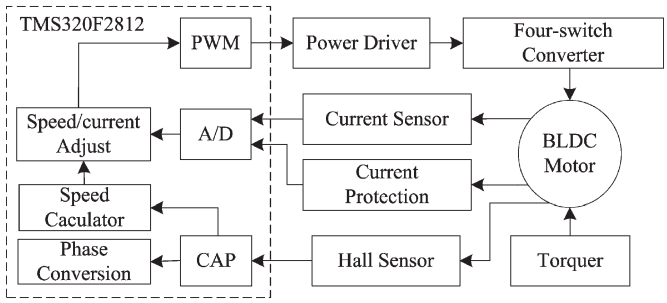

Fig. 14. Experimental system of the four-switch three-phase BLDC motor.

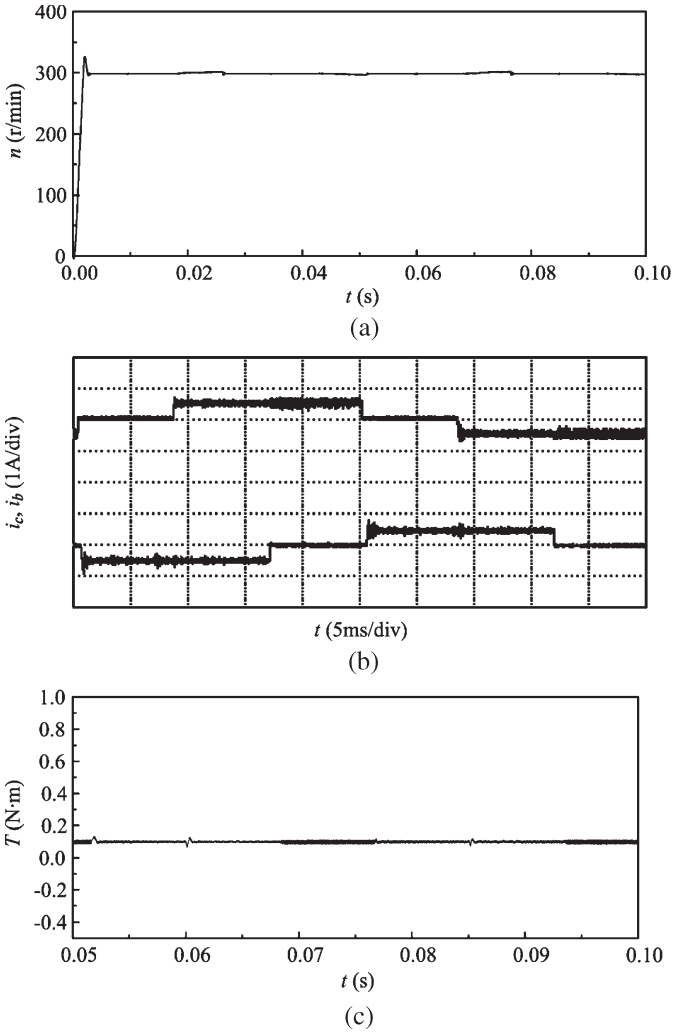

Fig. 15. Experimental waveforms in the situation of 300 r/min and 0.1 N · m when the motor is controlled by the single-current-sensor strategy. (a) Speed curve. (b) Current waveforms. (c) Torque curve.

Commutation torque ripples can be seen in both simulation and experimental results. Because of the trapezoidal back-EMF, the BLDC motor needs an ideal rectangular current to generate smooth instantaneous torque. It is not available in practice due to the winding inductance and finite inverter voltage. In the four-switch drive system, commutation torque ripples are even more severe unless a suitable current control strategy is adopted because the current flowing through the capacitor is difficult to control. Consequently, commutation torque ripples could not be eliminated but only reduced by motor design and current control method.

The whole system is implemented by the TMS320F2812 DSP. The configuration of the experimental system is shown in Fig. 14.

In the experimental setup, i_a and i_b cannot be sensed in modes 1 and 4, so that current overflowing cannot be monitored. A protective circuit consisting of current sampling resistance and voltage comparator being indicated as current

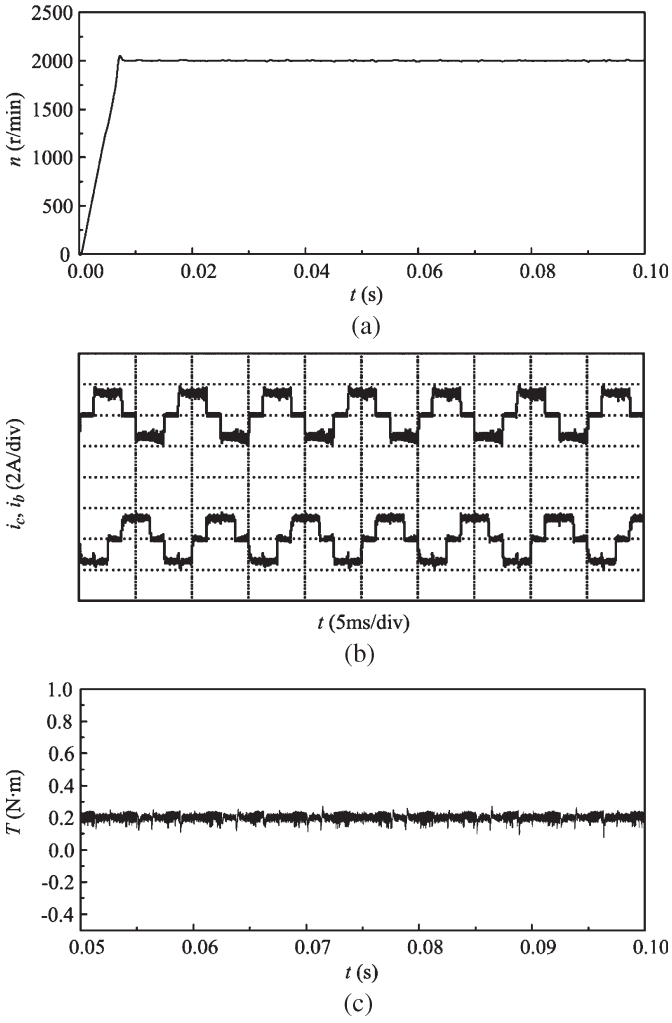

Fig. 16. Experimental waveforms in the situation of 2000 r/min and 0.2 N · m when the motor is controlled by the single-current-sensor strategy. (a) Speed curve. (b) Current waveforms. (c) Torque curve.

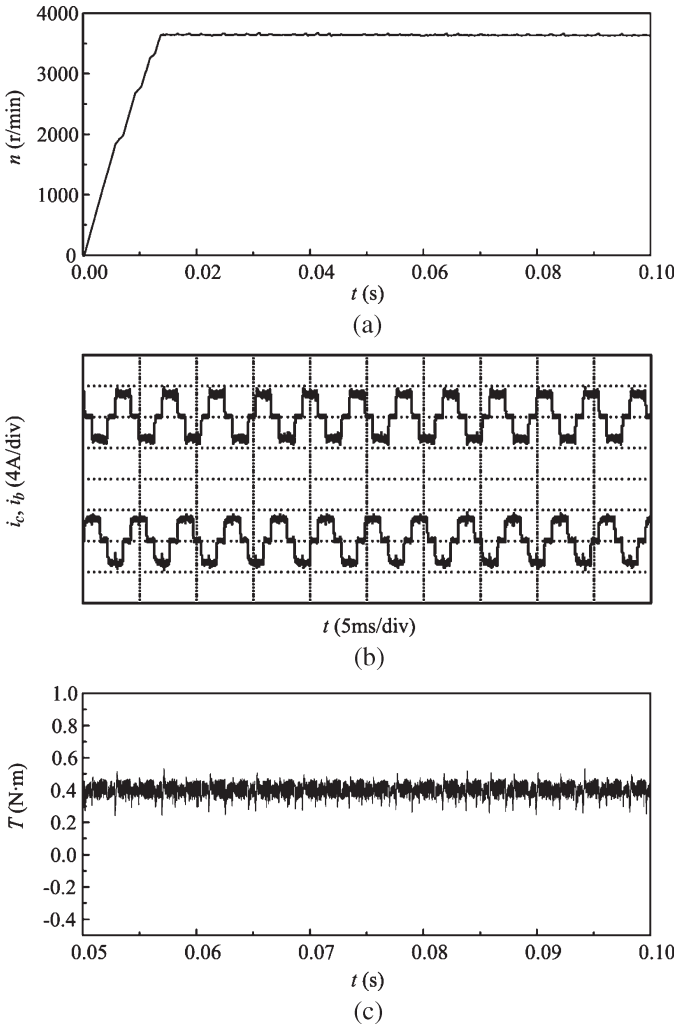

Fig. 17. Experimental waveforms in the situation of 3600 r/min and 0.4 N · m when the motor is controlled by the single-current-sensor strategy. (a) Speed curve. (b) Current waveforms. (c) Torque curve.

protection module in the diagram has been used as limitation approach for the drive safety issue in controller 2. In controller 3, freewheeling diodes provide discharging loop, and i_a and $-i_b$ will drop quickly without overflowing.

Figs. 15–17 show the phase current, torque, and speed waveforms when the motor works in the following situations: 1) 300 r/min and 0.1 N · m; 2) 2000 r/min and 0.2 N · m; and 3) 3600 r/min and 0.4 N · m.

From Figs. 15–17, it can be seen that whether working at low speed and under light load or at rated speed and under rated load, the motor performs satisfactorily. Phase current maintains rectangular waveforms, speed curve is stable, and torque has little fluctuation.

V. Conclusion

An advanced double-loop control strategy based on the four-switch topology for the BLDC motor drive has been proposed. A single-neuron adaptive PI controller is used by the outer loop to develop the performance of speed control. The algorithm is easy to implement on the microcontroller, and the cost of the whole system is lowered because only one current sensor is required. Finally, qualified performance was verified by simulation and experimental results under different work conditions, at different speeds, and under different loads.

It should be noted that reducing the quantity of current sensor surely brings some negative impacts to the control system, such as maximum current limitation in certain modes. Additionally, the program tends to be complicated because a special algorithm is necessary as compensation on the reduction of current sensor. Consequently, the software overhead is increased. For further research, how to improve system reliability and optimize software design should be the key point to implement the proposed strategy in industrial application.

References

[1] K.-W. Lee, D.-K. Kim, B.-T. Kim, and B.-I. Kwon, "A novel starting method of the surface permanent-magnet BLDC motors without position sensor for reciprocating compressor," *IEEE Trans. Ind. Appl.*, vol. 44, no. 1, pp. 85–92, Jan./Feb. 2008.

[2] D.-K. Kim, K.-W. Lee, and B.-I. Kwon, "Commutation torque ripple reduction in a position sensorless brushless DC motor drive," *IEEE Trans. Power Electron.*, vol. 21, no. 6, pp. 1762–1768, Nov. 2006.

[3] F. Rodriguez and A. Emadi, "A novel digital control technique for brushless DC motor drives," *IEEE Trans. Ind. Electron.*, vol. 54, no. 5, pp. 2365–2373, Oct. 2007.

[4] C.-W. Hung, C.-T. Lin, C.-W. Liu, and J.-Y. Yen, "A variable-sampling controller for brushless DC motor drives with low-resolution position sensors," *IEEE Trans. Ind. Electron.*, vol. 54, no. 5, pp. 2846–2852, Oct. 2007.
[5] S. Rajagopalan, J. M. Aller, J. A. Restrepo, T. G. Habetler, and R. G. Harley, "Analytic-wavelet-ridge-based detection of dynamic eccentricity in brushless direct current (BLDC) motors functioning under operating conditions," *IEEE Trans. Ind. Electron.*, vol. 54, no. 3, pp. 1410–1419, Jun. 2007.
[6] G. J. Su and J. W. Mckeever, "Low-cost sensorless control of brushless DC motors with improved speed range," *IEEE Trans. Power Electron.*, vol. 19, no. 2, pp. 296–302, Mar. 2004.
[7] C. T. Pan and E. Fang, "A phase-locked-loop-assisted internal model adjustable-speed controller for BLDC motors," *IEEE Trans. Ind. Electron.*, vol. 55, no. 9, pp. 3415–3425, Sep. 2008.
[8] L. Parsa and H. Lei, "Interior permanent magnet motors with reduced torque pulsation," *IEEE Trans. Ind. Electron.*, vol. 55, no. 2, pp. 602–609, Feb. 2008.
[9] D.-H. Jung and I.-J. Ha, "Low-cost sensorless control of brushless DC motors using a frequency-independent phase shifter," *IEEE Trans. Power Electron.*, vol. 15, no. 4, pp. 744–752, Jul. 2000.
[10] J.-H. Lee, S.-C. Ahn, and D.-S. Hyun, "A BLDCM drive with trapezoidal back EMF using four-switch three phase inverter," in *Conf. Rec. IEEE IAS Annu. Meeting*, 2000, vol. 3, pp. 1705–1709.
[11] S.-H. Park, T.-S. Kim, S.-C. Ahn, and D.-S. Hyun, "A simple current control algorithm for torque ripple reduction of brushless DC motor using four-switch three-phase inverter," in *Proc. IEEE Power Electron. Spec. Conf.*, 2003, vol. 2, pp. 574–579.
[12] Q. Fu, H. Lin, and H. T. Zhang, "Single-current-sensor sliding mode driving strategy for four-switch three-phase brushless DC motor," in *Proc. IEEE Ind. Technol. Conf.*, 2006, pp. 2396–2401.
[13] S. B. Ozturk, W. C. Alexander, and H. A. Toliyat, "Direct torque control of four-switch brushless DC motor with non-sinusoidal back-EMF," in *Proc. IEEE Power Electron. Spec. Conf.*, 2008, pp. 4730–4736.
[14] Z. J. Jiang, D. G. Xu, and F. P. Wang, "An improved development of four-switch low cost inverter on voltage equilibrium with magnetic flux control method," in *Proc. IEEE Elect. Mach. Syst. Conf.*, 2003, vol. 1, pp. 379–382.
[15] B.-K. Lee, T.-H. Kim, and M. Ehsani, "On the feasibility of four-switch three-phase BLDC motor drives for low cost commercial applications: Topology and control," *IEEE Trans. Power Electron.*, vol. 18, no. 1, pp. 164–172, Jan. 2003.
[16] J.-H. Lee, T.-S. Kim, and D.-S. Hyun, "A study for improved of speed response characteristic in four-switch three-phase BLDC motor," in *Proc. IEEE Ind. Electron. Soc. Conf.*, 2004, vol. 2, pp. 1339–1343.
[17] A. H. Niassar, A. Vahedi, and H. Moghbelli, "Analysis and control of commutation torque ripple in four-switch three-phase brushless DC motor drive," in *Proc. IEEE Ind. Technol. Conf.*, 2006, pp. 239–246.
[18] A. H. Niasar, H. Moghbeli, and A. Vahedi, "Adaptive neuron-fuzzy control with fuzzy supervisory learning algorithm for speed regulation of 4-switch inverter brushless DC machines," in *Proc. IEEE Power Electron. Motion Control Conf.*, 2006, pp. 1–5.
[19] C.-T. Lin, C.-W. Hung, and C.-W. Liu, "Position sensorless control for four-switch three-phase brushless DC motor drives," *IEEE Trans. Power Electron.*, vol. 23, no. 1, pp. 438–444, Jan. 2008.
[20] A. H. Niasar, H. Moghbeli, and A. Vahedi, "A novel sensorless control method for four-switch brushless DC motor drive without using any 30° phase shifter," in *Proc. IEEE Elect. Mach. Syst. Conf.*, 2007, pp. 408–413.
[21] M. H. Zhang, C. L. Xia, Y. Tian, and T. N. Shi, "Speed control of brushless DC motor based on single neuron PID and wavelet neural network," in *Proc. IEEE Control Autom. Conf.*, 2007, pp. 617–620.
[22] T. N. Shi, C. L. Xia, M. C. Wang, and Q. Zhang, "Single neural PID control for sensorless switched reluctance motor based on RBF neural network," in *Proc. IEEE Intell. Control Autom. Conf.*, 2006, vol. 2, pp. 8069–8073.

Changliang Xia (M'08) was born in Tianjin, China, in 1968. He received the B.S. degree in electrical engineering from Tianjin University, Tianjin, in 1990, and the M.S. and Ph.D. degrees in electrical engineering from Zhejiang University, Hangzhou, China, in 1993 and 1995, respectively.

He is currently a Professor with the School of Electrical Engineering and Automation, Tianjin University. His current research interests include electrical machines, power electronics, motor drives, and computer control.

Zhiqiang Li was born in Hebei, China, in 1981. He received the B.S. and M.S. degrees in electrical engineering from Tianjin University, Tianjin, China, in 2003 and 2005, respectively, where he is currently working toward the Ph.D. degree in electrical engineering in the School of Electrical Engineering and Automation.

His research interests include electrical machines and motor drives.

Tingna Shi was born in Zhejiang, China, in 1969. She received the B.S. and M.S. degrees in electrical engineering from Zhejiang University, Hangzhou, China, in 1991 and 1996, respectively.

She is currently an Associate Professor with the School of Electrical Engineering and Automation, Tianjin University, Tianjin, China. Her current research interests include electrical machines, power electronics, and computer control.